# EFFICIENT DEBLENDING USING MEDIAN FILTERING WITHOUT CORRECT NORMAL MOVEOUT - WITH COMPARISON TO MIGRATED IMAGES

MIN BAI and JUAN WU

*School of Resources and Environment, North China University of Water Resources and Electric Power, Zhengzhou 450045, P.R. China. baimin@ncwu.edu.cn*

(Received December 12, 2016; revised version accepted August 1, 2017)

ABSTRACT

Bai, M. and Wu, J., 2017. Efficient deblending using median filtering without correct normal moveout - with comparison to migrated images. *Journal of Seismic Exploration*, 26: 455-479.

The benefits of simultaneous source acquisition are compromised by the challenges of dealing with intense blending noise. While the median filtering approach can be effectively used in attenuating blending interference due to its superb performance in rejecting spiky noise, it requires two or three times of normal moveout (NMO) based velocity analysis in order to exactly flatten the seismic data and thus it is computationally expensive. In this paper, we propose an efficient deblending framework that is based on a modified median filtering approach and does not require a correct NMO correction. The modified median filtering approach depends on a novel median filter that can spatially change the filter length and can deal with curved events due to the incorrect NMO. The median filter with variable window length is an adaptive median filter, thus it can be conveniently used in the presented processing workflow without the need of much human input. We not only compare the deblending performance in the data space, but also present detailed comparison in the image space. An important criterion we use to compare the deblending performance is the local correlation between deblended data and removed blending noise. The whole deblending workflow aims at minimizing the local correlation coefficients. Numerical synthetic and field data examples confirm the speedup of the proposed method without sacrificing the deblending performance.

KEY WORDS: deblending, median filtering, normal moveout migration.

0963-0651/17/$5.00 

## INTRODUCTION

The simultaneous-source acquisition refers to the newly developed acquisition technique that fires more than one shots at nearly the same time regardless of their interference. In conventional acquisition, either the temporal shooting intervals or the spatial sampling intervals are large enough so that the interference between successive shots can be left out. Thus, the novel technique can reduce the acquisition period and at the same time can improve the data quality because of the significantly decreased spatial sampling interval (Wood, 1974; Garotta, 1983; Martinez and Crews, 1987; Womack and Cruz, 1988; Ward et al., 1990; Werner, 1993; Beasley et al., 1998; Ikelle et al., 2000; Moerig et al., 2002; Beasley, 2008; Moore et al., 2008; Spitz et al., 2008; Berkhout, 2008; Moore, 2010; Mahdad et al., 2011; Beasley et al., 2012; Mahdad, 2012; Qu et al., 2015, 2016; Xue et al., 2016a, 2017).

The profound benefits of simultaneous sources, which are compromised by the blending interference generated from adjacent sources (Wapenaar et al., 2012), have attracted much attention (Abma et al., 2010, 2012; Abma, 2014; Berkhout et al., 2012; Chen et al., 2014a, 2015; Hampson et al., 2008; Mahdad et al., 2012; Qu et al., 2014; Zu et al., 2016b; Zhou et al., 2017; Chen et al., 2017a). There are two main categories to deal with the blended interference. The first category is to separate the blended data as the conventional seismic data for the subsequent seismic processes, which is called "deblending". Deblending is currently the dominant way to process simultaneous sources data and there are a lot of successful field applications reported in the literature. The second category is direct imaging and inversion without deblending, which do not require the dithering schedule. Recently, some researchers indeed get some good results on simultaneous sources by directly imaging and inversion (Berkhout et al., 2012; Choi and Alkhalifah, 2012; Guitton and Daz, 2012; Xue et al., 2016c; Chen et al., 2015; Zhang et al., 2016b; Ren and Tian, 2016; Shen et al., 2016; Gan et al., 2016e; Ebrahimi et al., 2017; Chen et al., 2017b). However, few successful field data tests using those direct imaging algorithms have been reported.

The deblending can be posed as a problem of noise attenuation or filtering (Liu et al., 2015; Gan et al., 2015a; Xue et al., 2016b; Liu et al., 2016b,f,d; Gan et al., 2016c,b; Huang et al., 2016, 2017b), which can then be solved by the prediction based method s (Liu et al., 2011; Liu and Chen, 2013), sparse transform based methods (Chen et al., 2016; Chen, 2016; Li et al., 2016c; Liu et al., 2016a; Sun and Wang, 2016; Wu et al., 2016; Kong et al., 2016; Siahsar et al., 2017; Chen, 2017), decomposition based methods (Chen and Ma, 2014; Yang et al., 2015a; Liu et al., 2016c; Ikelle, 2016; Chen et al., 2017c), morphological operation based methods (Li et al., 2016a,b), inversion and optimization based approaches (Chen and Fomel, 2015; Chen and Jin, 2015). Mahdad et al. (2011) utilize the least-squares deblended data to estimate the

blending noise and apply a threshold in common receiver domain to subtract it from the blended data. Chen et al. (2014b) implement the simplest form of median filtering to separate the blended data by flatting the common mid-point (CMP) gathers with two or three times of iterative normal-moveout (NMO) velocity analysis. Huo et al. (2012) extend the well-known conventional median filter from a scalar implementation to a vector median filter that can separate the blended CMP gathers without requiring the NMO. Gan et al. (2016d) develop a novel structure-oriented median filter that is applied along the local structure direction. Kim et al. (2009) simulate the noise model from the blended record and then adaptively subtracts the blended interference by matching the noise model and the blended interference. Another way for deblending is inversion. Inversion methods treat the separation problem as an estimation problem, which is ill-posed, so the regularization item is required to obtain a stable estimation (Ikelle, 2007; Akerberg et al., 2008; Lin and Herrmann, 2009; Doulgeris et al., 2012; Chen et al., 2014a; Qu et al., 2014; Zhang et al., 2016a; Zu et al., 2016b,a). The inversion based deblending approach has been demonstrated to perform better than the filtering based approach but at the expense of significantly more expensive computational cost than the inversion based approach. Chen (2015b) propose a robust iterative deblending method with multiple constraints (i.e., sparsity and orthogonality) for dealing with more complicated data structures. Zhou (2017) propose a similar multiple-constraints regularized iterative framework by constructing a blending mask from the blending schedule based on the POCS framework.

Following Chen et al. (2014b), we are investigating a more efficient median filtering based deblending approach. The velocity analysis required by correct NMO (CNMO) is not necessary in the newly developed deblending framework, where a novel median filtering approach is applied to cope with curved events due to imperfect NMO correction. In the proposed deblending framework, a pseudo-NMO (PNMO) with a rough NMO velocity is adequate to guarantee a successful deblending performance. The median filter with variable window length is a fully adaptive filtering method that can be conveniently used in the presented framework without troublesome human input. We introduce the algorithm steps in detail and confirm the deblending performance in both data space and image space via one synthetic and one field data examples.

## METHOD

### Data transformation

The crosstalk noise is coherent in common shot gathers and is incoherent in common receiver and offset gathers. For better spatial coherency in order to apply a median filter, the field data is first transformed from shot-receiver

domain to midpoint-offset domain.

The transformation from shot-receiver domain to midpoint-offset domain can be realized by the following equations:

$$\mathbf{m} = (\mathbf{s} + \mathbf{r})/2 \quad , \tag{1}$$

$$\mathbf{h} = (\mathbf{r} - \mathbf{s})/2 \quad , \tag{2}$$

where **m**, **s** and **r** denote the coordinates of midpoint, shot, and receiver, respectively. **h** denotes the offset.

## Median filtering with a fixed window length

A median filter can be used to obtain an excellent job in rejecting impulse (spiky) noise, which has extreme value compared with neighbor values. Compared with the commonly known smoothing filter, the median filter enjoys several advantages.

- The median filter is better in preserving edges because each output value for the data points are one of the neighbor values. Different from the mean filter (Yang et al., 2015b), the median filter will not create unrealistic values near the boundaries (edges).

- The median filter is less sensitive to extreme values. Instead of calculating a contribution from these extreme values in a mean filter, the median filter simply remove these extreme values.

- The median filter can be applied repeatedly because of the smaller damages it causes to edges. In the contrary, the mean filter will cause much more damages to the data structure.

Given a 1D signal, to implement a median filter, the following two steps are taken:

1. For each data point in the 1D signal, creating a local window with fixed window length L. The window is composed of the current processing point and its neighboring points.

2. Selecting the median of each local window and use this median value as the output value of the current processing point.

Given a 2D signal, a 1D median filter is applied along the spatial direction and it is implemented for each row of the waveform matrix one by

one. Mathematically, a median filter can be expressed using the following formula when applied to a 2D signal.

$$\hat{u}_{i,j} = \arg \min_{u_m \in U_{i,j}} \sum_{l=1}^{L} \| u_m - u_l \|_1 \ ,$$

where $\hat{u}_{i,j}$ is the output value for location $x_{i,j}$. $U_{i,j} = \{u_1, u_2, \ldots, u_L\}$, i,j are the position indices in a 2D profile, $l$ and m are both indices in the filtering window. L is the length of the filtering window.

Fig. 1 shows an example in which a median filter is applied to a seismic data with flattened events. Fig. 1a shows the noisy data before applying median filtering and Fig. 1b shows the denoised data using median filtering. The median filtering successfully reject all spiky noise without damaging the useful signals.

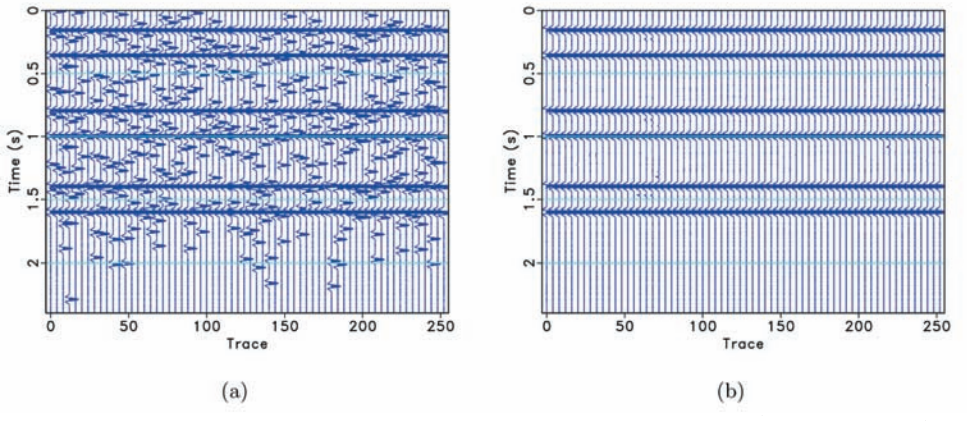


Fig. 1. Demonstration of median filtering in the case of exact flattening.

## Median filtering with a variable window length

The effective performance of the median filtering depends on the exactly flattened events. When the events are not flattened, the traditional median filtering will damage a lot of useful energy. Fig. 2 show an example of median filtering where the data contains both flattened and unflattened events. It is obvious that the median filtering causes a serious damage to the unflattened energy.

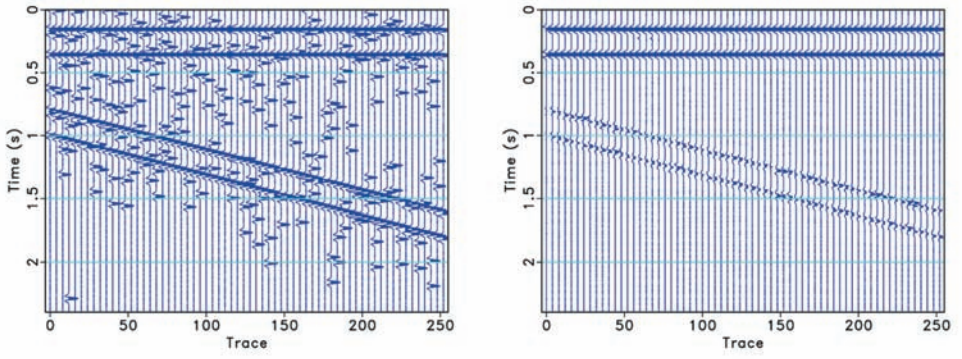


Fig. 2. Demonstration of median filtering in the case of imperfect flattening. (a) Data before median filtering. (b) Data after median filtering with fixed window length.

In order to deal with unflattened events and preserve useful energy as much as possible, we can use a variable window length strategy. In the modified median filtering, L becomes $L_{i,j}$, varying with respect to location $x_{i,j}$. The new filtering expression is:

$$\hat{v}_{i,j} = \arg \min_{v_m \in U_{i,j}} \sum_{l=1}^{L_{i,j}} \| v_m - v_l \|_p \quad , \tag{3}$$

where $\hat{v}_{i,j}$ is the output value for location $x_{i,j}$ after applying the modified median filter, $U_{i,j} = \{v_1, v_2, \ldots, v_{L_{i,j}}\}$. The filter length $L_{i,j}$ can be chosen based on the criterion that is similar to Liu et al. (2009).

$$L_{i,j} = \begin{cases} L + l_1, & 0 \le |s^L_{i,j}| \le s_1 \\ L + l_2, & s_1 < |s^L_{i,j}| < s_2 \\ L, & s_2 \le |s^L_{i,j}| \le s_3 \\ L - l_3, & s_3 < |s^L_{i,j}| < s_4 \\ L - l_4, & s_4 \le |s^L_{i,j}| \le s_{max} \end{cases} , \tag{4}$$

where $l_1, l_2, l_3, l_4$ are predefined parameters corresponding to the increments or decrements for the length of filter window and are generally chosen as 4,2,2,4 in default, respectively; $s^L_{i,j}$ is the signal reliability (SR), which can be defined as the local similarity (Fomel, 2007) between the initially filtered data $u^L_{i,j}$ with a window length L and the original data $u_{i,j}$ for point $x_{i,j}$:

$$s^{L}_{i,j} = \mathbf{S}[u^{L}_{i,j}, u_{i,j}] \quad . \tag{5}$$

Here, $\mathbf{S}[\mathbf{x}, \mathbf{y}]$ denotes the local similarity between $\mathbf{x}$ and $\mathbf{y}$. $s_1$, $s_2$, $s_3$, and $s_4$ are four thresholds, and are empirically chosen as $s_1 = 0.15s_{max}$, $s_2 = 0.25s_{max}$, $s_3 = 0.75s_{max}$, and $s_4 = 0.85s_{max}$. $s_{max}$ denotes the maximum value of the similarity map (Chen, 2015a).

Applying the modified median filtering in the imperfectly flattened gathers, we can preserve much useful energy that remains not flattened. Fig. 3 shows a demonstration on how the median filter with variable window length can help preserve the unflattened energy.

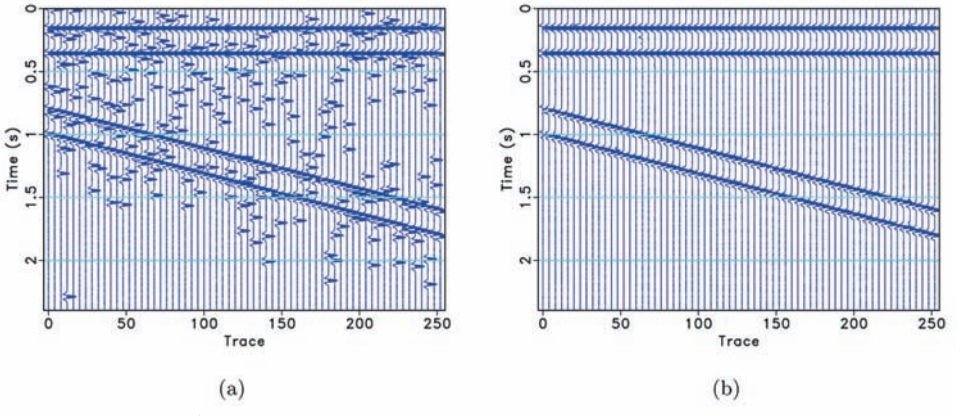


Fig. 3. Demonstration of median filtering with variable window length in the case of imperfect flattening. (a) Data before median filtering. (b) Data after median filtering with variable window lengths.

## Performance evaluation using local correlation

The eventual goal of spiky noise attenuation is to maximize the noise removal and signal preservation. For evaluating the deblending performance, we need to define a quantitative measure. The main target of the whole processing workflow which will be discussed later (e.g., NMOs, stack, domains, multiple runs, etc.) is to minimize the numerical measure. For synthetic example, since we know the exact solution, we can use the following signal- to-noise ratio (SNR) measurement (Gan et al., 2015b; Liu et al., 2016e; Gan et al., 2016a; Zhong et al., 2016; Huang et al., 2017a):

$$\mathrm{SNR} = 10\log_{10}(\|\mathbf{s}\|_2^2 / \|\mathbf{s} - \hat{\mathbf{s}}\|_2^2) \quad , \tag{6}$$

where $\mathbf{s}$ and $\hat{\mathbf{s}}$ are exact signal and deblended signal, respectively. The SNR measure is only valid for synthetic example, since we have the ground truth. For field data example, we do not know the true signal. In order to numerically measure the denoising performance, we define the local correlation coefficient for such purpose:

$$\gamma_w(t) = \sum_{i=t-w/2}^{t+w/2} \mathbf{a}_i\mathbf{b}_i \Big/ \sqrt{\Big\{ \sum_{i=t-w/2}^{t+w/2} \mathbf{a}_i^2 \sum_{i=t-w/2}^{t+w/2} \mathbf{b}_i^2 \Big\}} \quad , \tag{7}$$

where w is window length. $\mathbf{a}$ and $\mathbf{b}$ are to input vectors for the calculation. $\gamma_w(t)$ denotes local correlation coefficients. The local correlation is a localized version of the commonly known global correlation coefficient, which is often widely used for calculating the correlation coefficient (or similarity) between two vectors. The global uncentered correlation coefficient between two discrete signals $\mathbf{a}_i^2$ and $\mathbf{b}_i^2$ can be defined as the functional

$$\gamma = \sum_{i=1}^{N} \mathbf{a}_i\mathbf{b}_i \Big/ \sqrt{\Big\{ \sum_{i=1}^{N} \mathbf{a}_i^2 \sum_{i=1}^{N} \mathbf{b}_i^2 \Big\}} \quad , \tag{8}$$

where N is the length of a signal. $\gamma$ denotes global correlation coefficient.

An example of local correlation is shown in Fig. 4. Fig. 4a shows the removed noise using median filter after exact flattening. Fig. 4b shows the local correlation between removed noise and denoised data. Another example is shown in Fig. 5, where the event is not flattened well. Fig. 5a shows the removed noise using median filter after imperfect flattening. Fig. 5b shows the removed noise using median filter with variable window length after imperfect flattening. Fig. 5a shows serious signal damage while the signal damage in Fig. 5b is much smaller since we can only observe a small amount of spatially coherent signal. Figs. 5c and 5d show the local correlation maps corresponding to Figs. 5a and 5b, respectively. We can observe clearly that the local correlation map effectively detect where we lose useful signals. With this criterion, we can compare the denoising performance of different methods even in the case of field data applications.

## Efficient deblending without correct normal moveout

In the proposed new deblending framework, the correct NMO is not required. Instead, we need apply median filtering twice. The first median filtering is applied with a fixed window length while the second median filtering is applied with a variable window length.

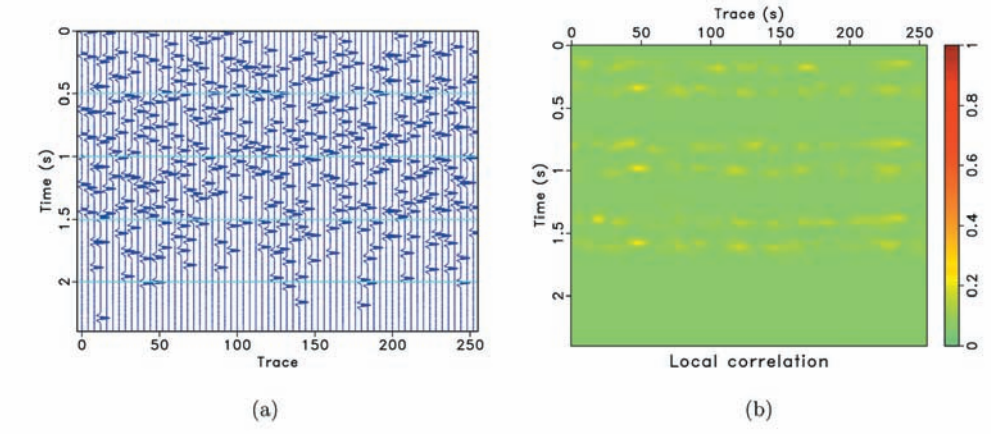


Fig. 4. (a) Removed noise using median filter after exact flattening. (b) Local correlation between removed noise and denoised data.

As a comparison, we first outline the algorithm framework of the traditional median filtering based deblending approach as follows:

1. Transform the blended data from CSG to CMG.
2. Apply velocity scan and pick the NMO velocity.
3. Apply normal moveout to raw blended records.
4. Apply median filtering along the offset direction in CMG.
5. Apply inverse normal moveout.
6. Iterate steps 2-5 by two or three times.

The efficient deblending framework is shown as follows:

1. Transform the blended data from CSG to CMG.
2. Apply a pseudo-NMO with a rough NMO velocity.
3. Apply the first median filter with a fixed window length along the offset direction in CMG.
4. Apply median filtering with variable window length along the offset direction in CMG.
5. Apply inverse normal moveout.

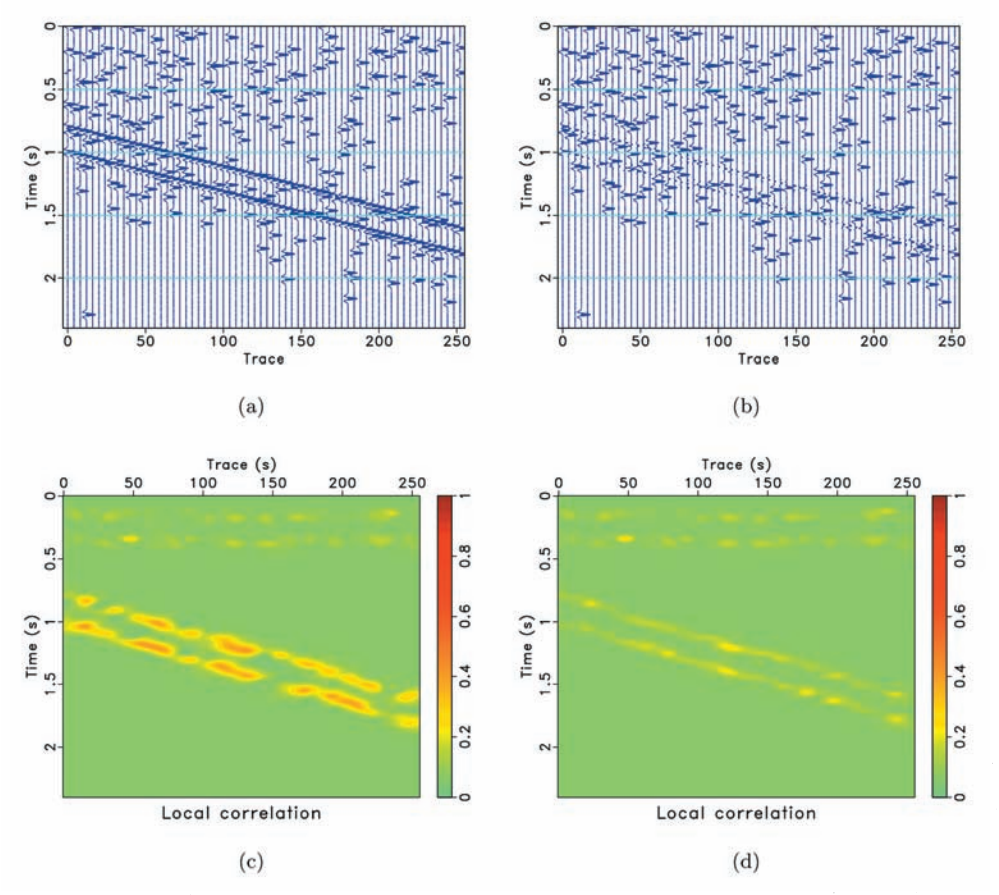


Fig. 5. (a) Removed noise using median filter after imperfect flattening. (b) Removed noise using median filter with variable window length after imperfect flattening. (c) Local correlation between removed noise and denoised data corresponding to (a). (d) Local correlation between removed noise and denoised data corresponding to (b).

## EXAMPLE

In this section, we use two examples to demonstrate the speedup and effectiveness of the proposed method. We compare the deblending performance in both data and image domains. The first example is a numerically blended synthetic example. Fig. 6 is a comparison of different data sets. Fig. 6a show the unblended data in common midpoint domain. Fig. 6b shows the blended data, which is highly corrupted by the intense blending interference. Fig. 6c shows the deblended result using the proposed method and Fig. 6d shows the

deblended data using the traditional median filtering based approach. It is salient that both deblending methods are very successful. All the blending interference are rejected while all useful signals are preserved very well. Note that to obtain such similar performance, it takes 248 seconds for the traditional method and it takes only 21 seconds for the proposed method. It is worth noting that most of the computation time is due to the NMO based velocity analysis.

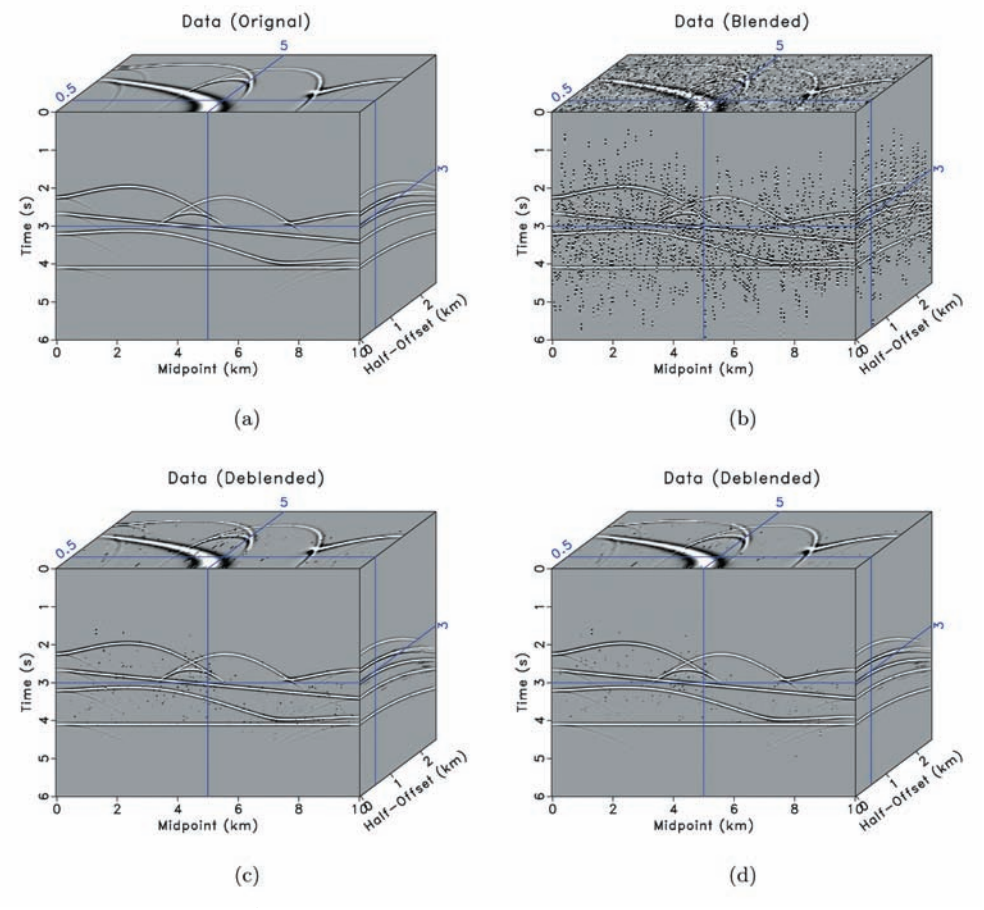


Fig. 6. Comparison of CMP gathers. (a) Original unblended CMP gathers. (b) Blended CMP gathers. (c) Deblended CMP gathers using PNMO-MF. (d) Deblended CMP gathers using CNMO-MF.

Then we evaluate the denoising performance by checking the noise cubes of different methods. The noise cubes are the difference between deblended data and removed noise. The noise cubes corresponding to different methods are

shown in Figs. 7a (PNMO-MF) and 7b (CNMO-MF), respectively. Figs. 7c and 7d show their corresponding local correlation cubes. It seems that both methods obtain very small local correlation, indicating that both methods obtain successful performance. We also plot a comparison of the average spectrum of all the traces for different data in Fig. 8. The black line denotes the average spectrum of clean data. The red line corresponds to blended data. The pink line corresponds to PNMO-MF method. The blue line corresponds to the CNMO-MF method. It is worth mentioning that the frequency band of the noise is the same as the useful signal. Deblending removes a large portion of the noise energy in the spectrum. Deblended data by two methods are almost the same in the spectrum.

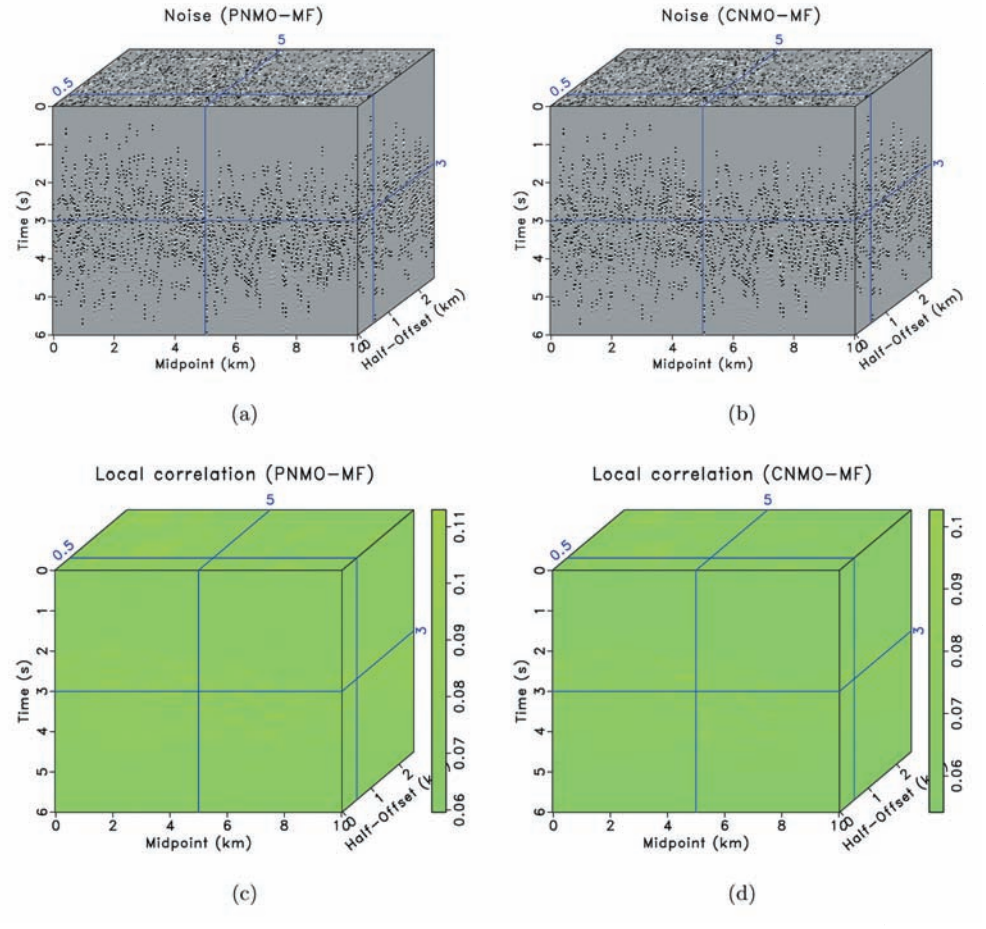


Fig. 7. (a) Noise cube using PNMO-MF. (b) Noise cube using CNMO-MF. (c) Local correlation between deblended data and removed noise using PNMO-MF. (d) Local correlation between deblended data and removed noise using CNMO-MF.

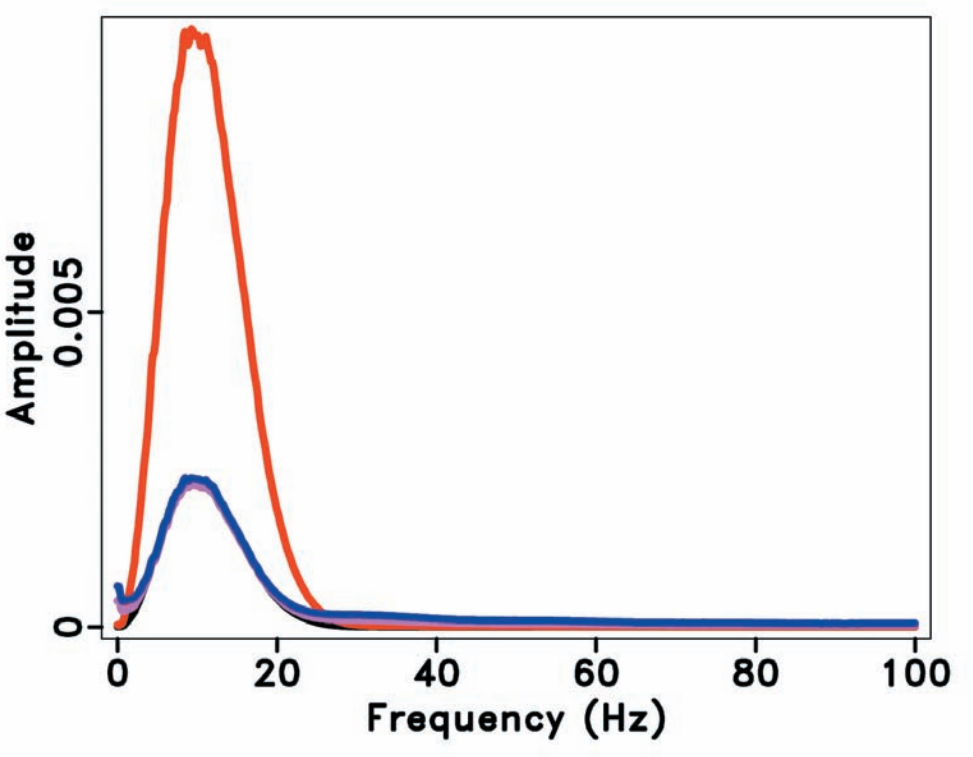


Fig. 8. Comparisons of the average spectrum of all the traces. The black line denotes the average spectrum of clean data. The red line corresponds to blended data. The pink line corresponds to PNMO-MF method. The blue line corresponds to the CNMO-MF method. Note that the frequency band of the noise is the same as the useful signal. Deblending removes a large portion of the noise energy in the spectrum. Deblended data by two methods are almost the same.

We further compare the migrated images of different datasets and show the results in Fig. 9. Fig. 9a shows the migrated image of unblended data using prestack Kirchhoff time migration (PSKTM) method. Fig. 9b shows the migrated image of blended data using PSKTM method. It can be seen from Fig. 9b that the blending interference causes extremely strong migration artifacts in the final image. Figs. 9c and 9d demonstrate the migrated images of the deblended data using the proposed and traditional methods, respectively. The migrated images in Figs. 9c and 9d are almost the same, and are much cleaner than the migrated image from blended data. This test demonstrates that the proposed method can obtain a similar deblending result and a corresponding migration image as the traditional method, but at a very low cost.

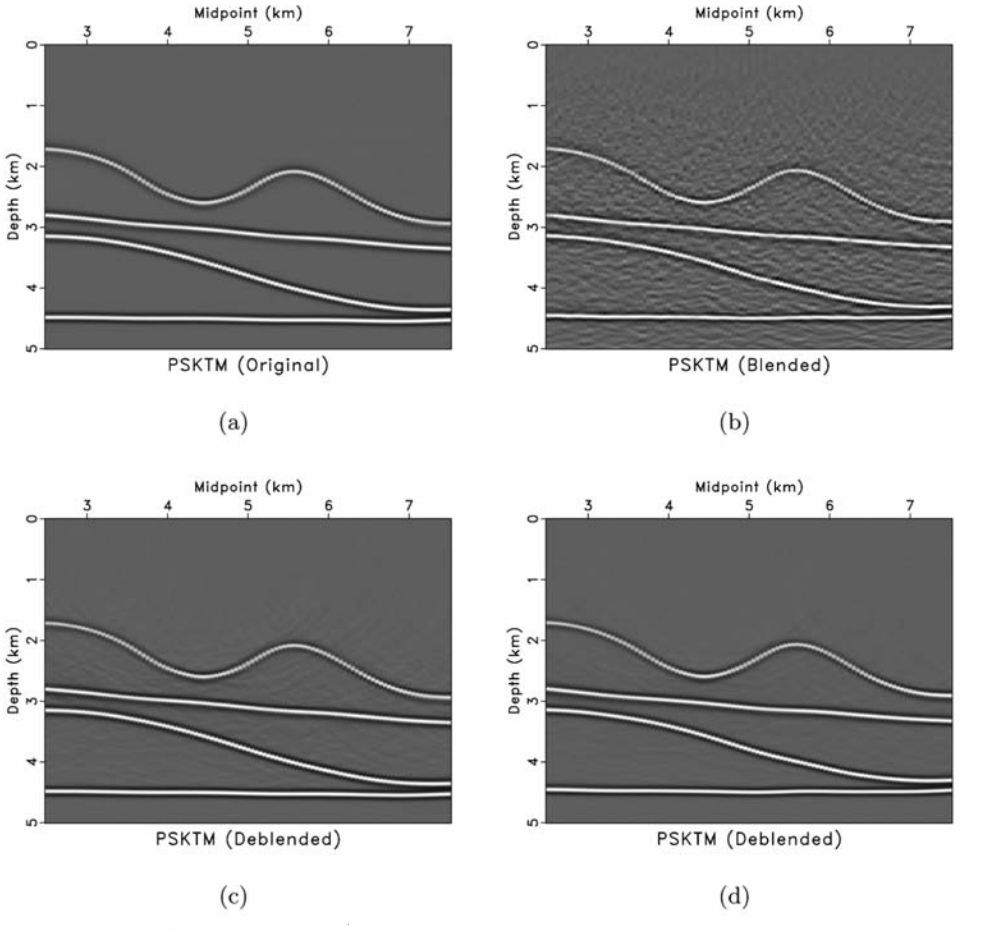


Fig. 9. Comparison of migration results. (a) Migrated result of unblended data. (b) Migrated result of blended data. (c) Migrated result of deblended data using PNMO-MF. (d) Migrated result of deblended data using CNMO-MF.

We then use a numerically blended field data set to further demonstrate the performance. Fig. 10 shows the original seismic record and blended seismic record in shot-offset domain. In order to apply the median filtering method, we first transform the data from shot domain to midpoint domain, and the blended data in the common midpoint domain is shown in Fig. 11. It is obvious that the blended data is extremely noisy due to the strong crosstalk caused by simultaneous shooting. Fig. 12 shows a comparison of deblended data using two methods in common midpoint domain. Fig. 13 shows a comparison of two deblended data in common shot domain, which confirms that both the deblending

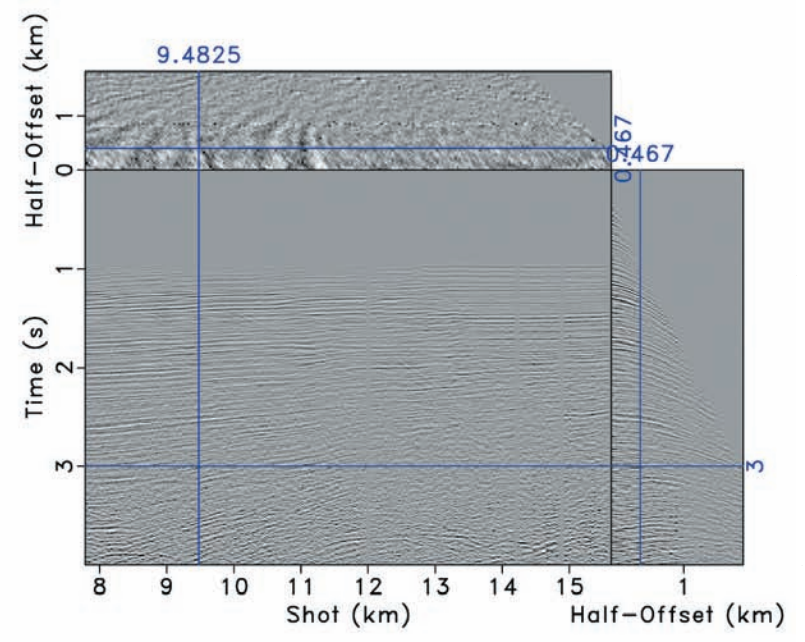


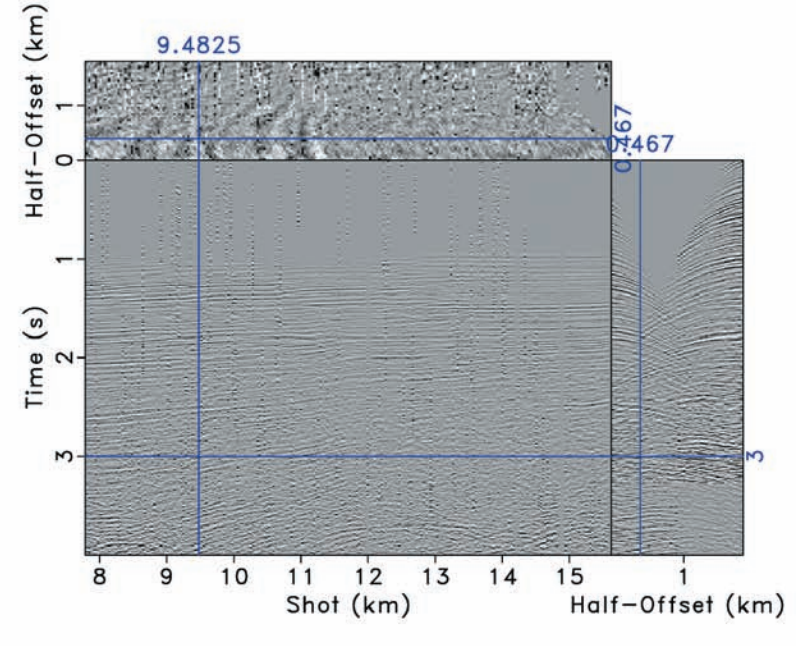


Fig. 10. (a) Gulf of Mexico dataset. (b) Blended data in time-shot-offset (TSO) domain.

methods are very successful. While both methods obtain almost the same performance, the proposed method obtains a computational speedup of more than 10 times. The detailed comparison of computing time is provided in the second row of Table 1. Fig. 14 shows the migration results of different data sets. Figs. 14a-14d correspond to the unblended data, blended data, deblended data using the proposed method, and deblended data using the traditional method, respectively. We also zoom a portion from the migration images of different data sets and show them in Fig. 15 for better comparison. The migrated images of two deblended data are both very close to that of the unblended data and contains much less artifacts than that of the blended data.

Table 1. Comparison of computational time between traditional and proposed deblending framework. In this comparison, two NMO velocity analysis are applied in the traditional approach.

| Test | Synthetic example | Field data example |
|---|---|---|
| Time of traditional framework (s) | 248 | 837 |
| Time of proposed framework (s) | 21 | 65 |

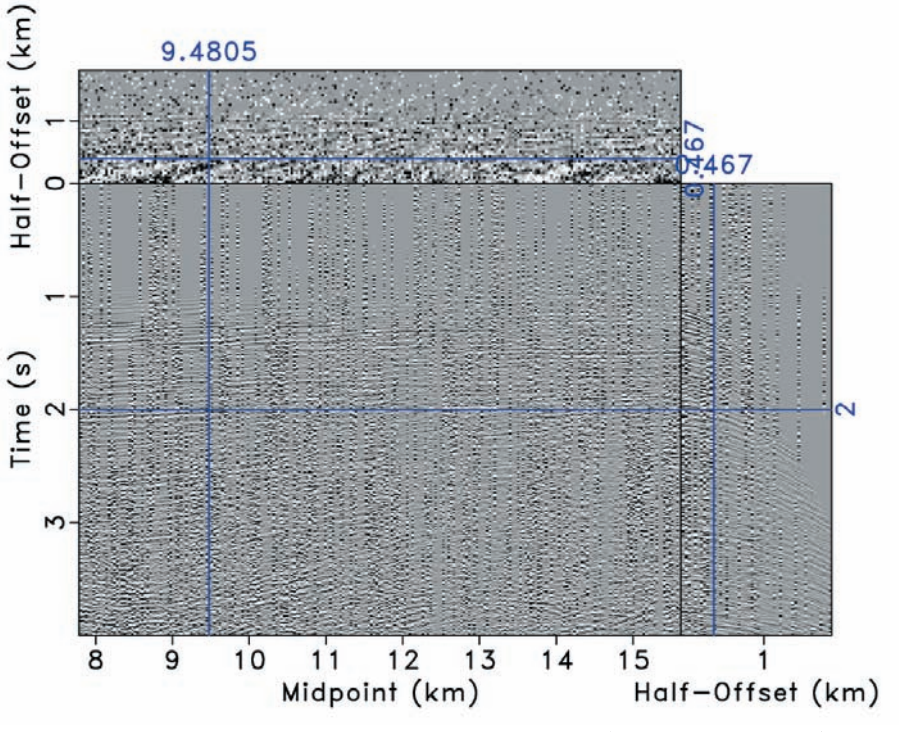


Fig. 11. (a) Blended data in time-midpoint-offset (TMO) domain.

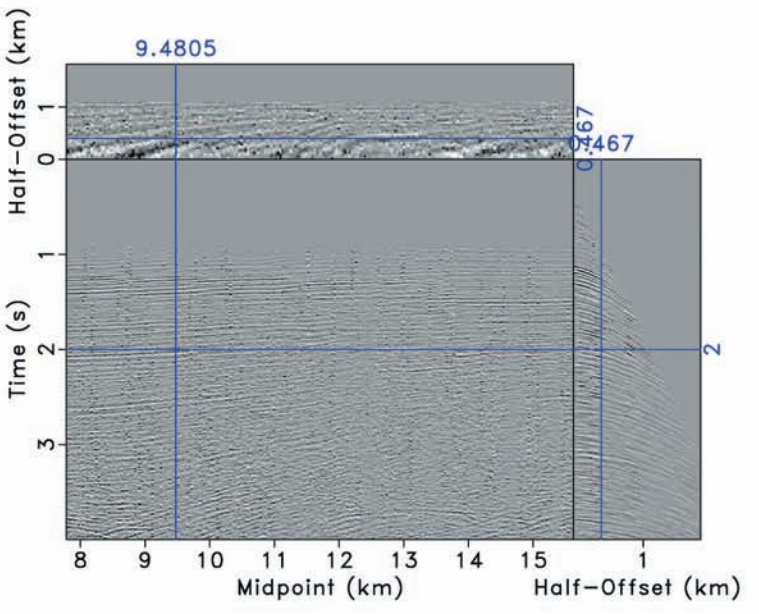


(a)

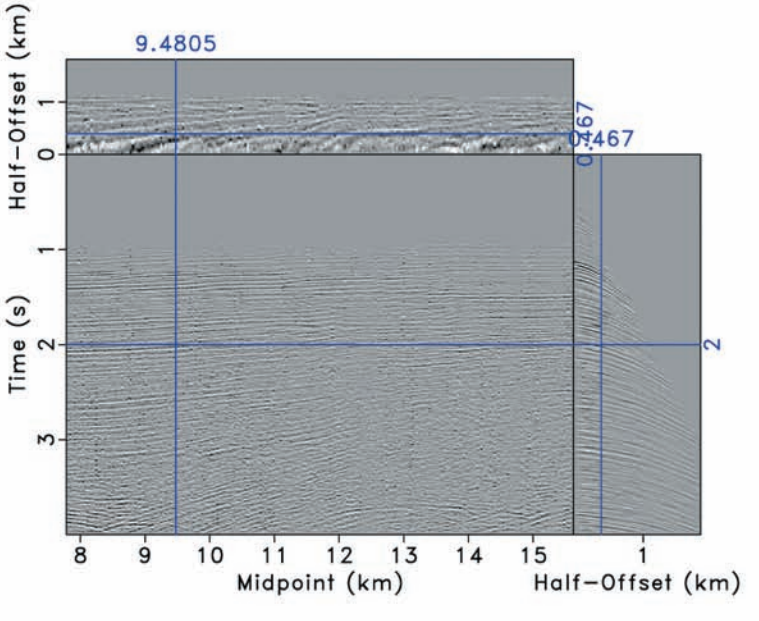


(b)

Fig. 12. (a) Deblended data in time-midpoint-offset (TMO) domain using PNMO-MF. (b) Deblended data in time-midpoint-offset (TMO) domain using CNMO-MF.

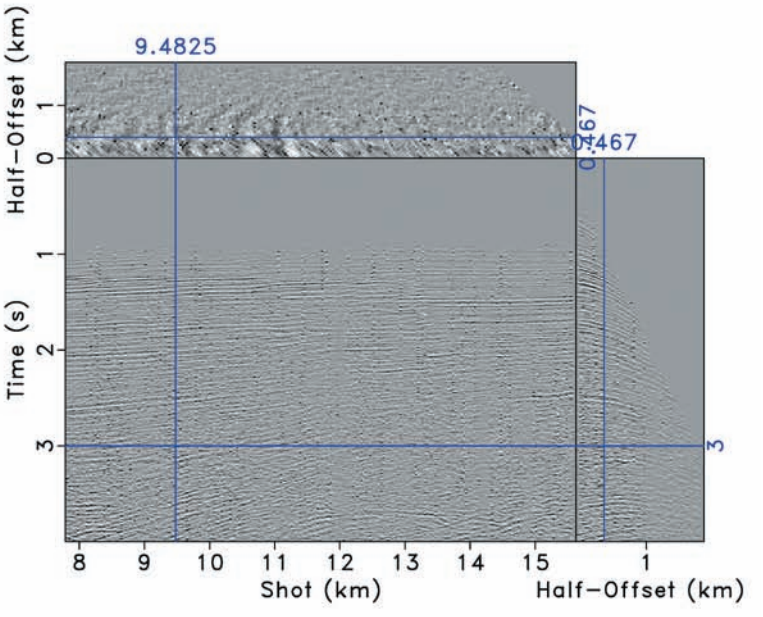


(a)

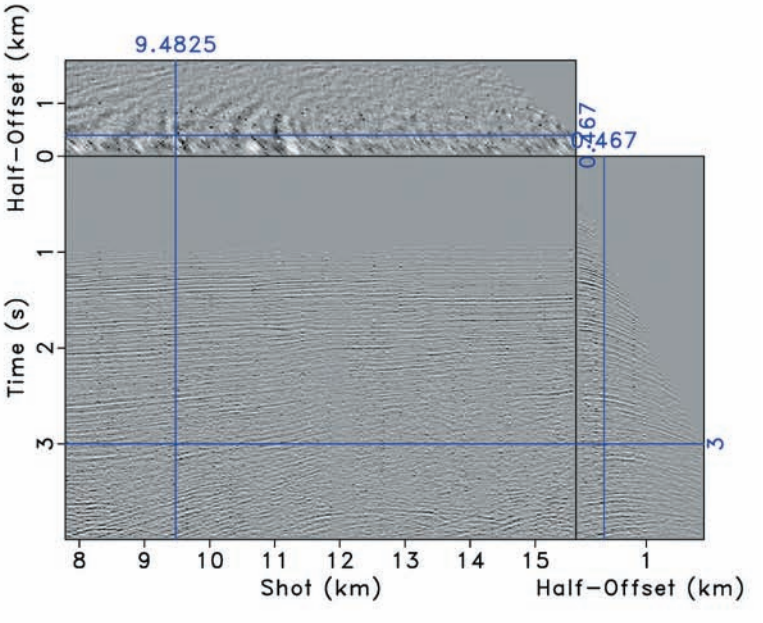


(b)

Fig. 13. (a) Deblended data in time-shot-offset (TSO) domain using PNMO-MF. (b) Deblended data in time-shot-offset (TSO) domain using CNMO-MF.

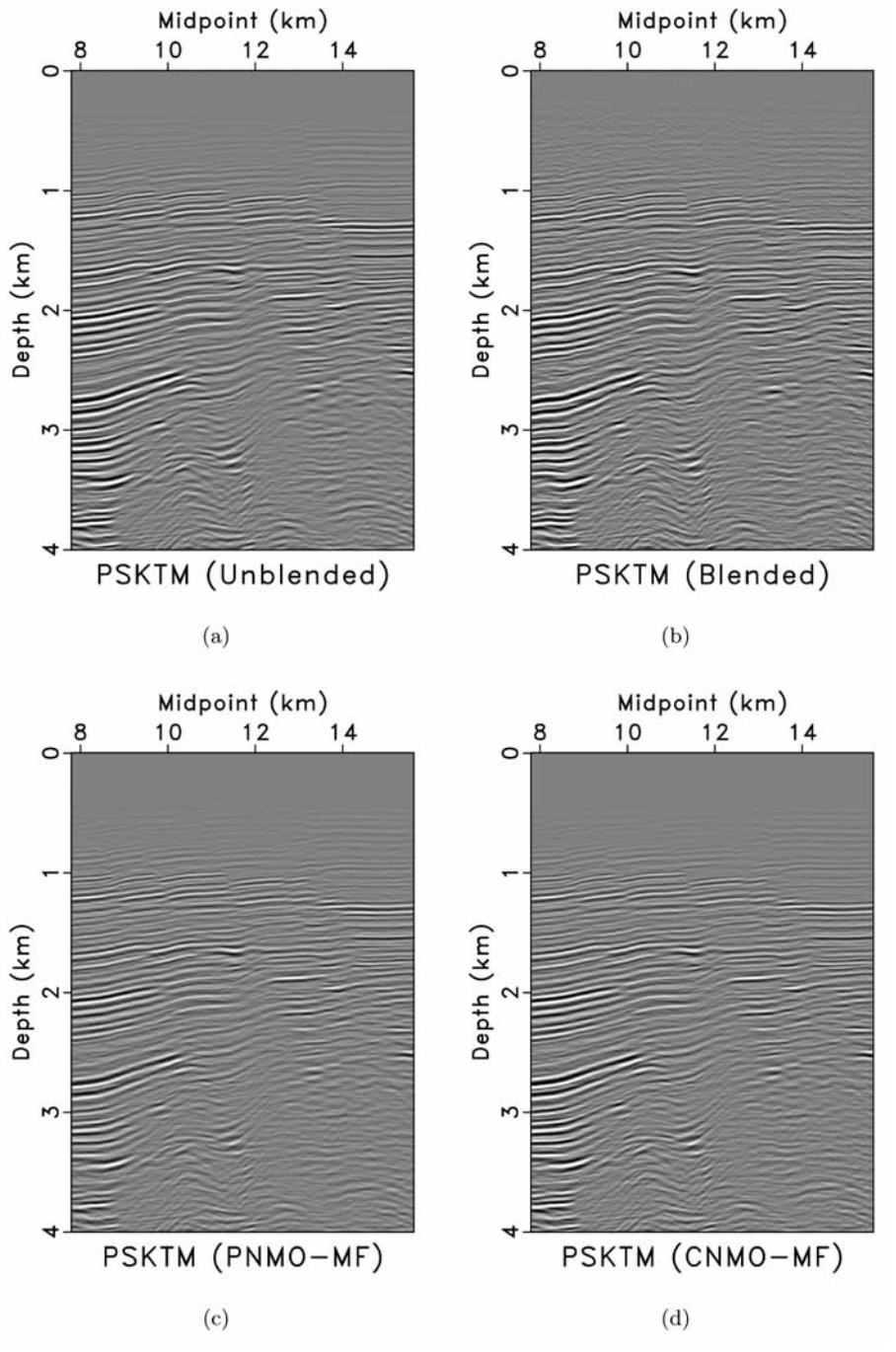


Fig. 14. Comparison of migration results. (a) Migrated result of unblended data. (b) Migrated result of blended data. (c) Migrated result of deblended data using PNMO-MF. (d) Migrated result of deblended data using CNMO-MF.

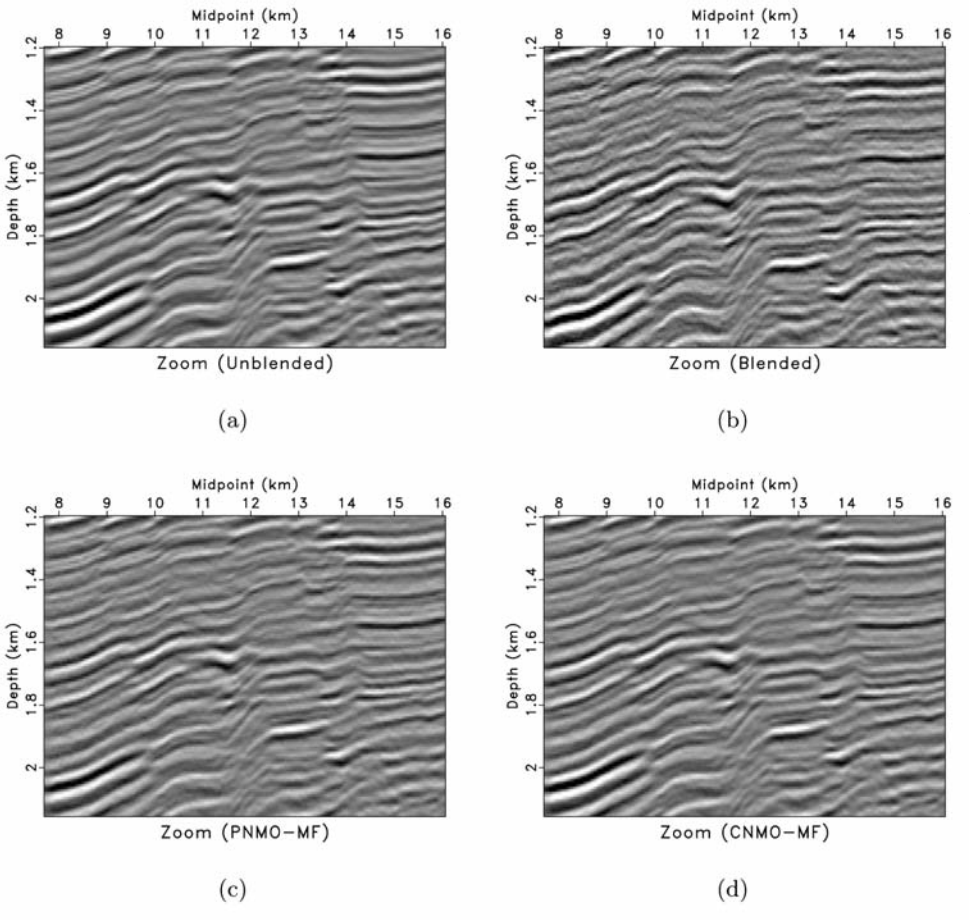


Fig. 15. Zoomed comparison of migration results. (a) Migrated result of unblended data. (b) Migrated result of blended data. (c) Migrated result of deblended data using PNMO- MF. (d) Migrated result of deblended data using CNMO-MF.

## CONCLUSIONS

We have outlined an efficient deblending framework that is based on a median filter that has a spatially variable filtering window length. The traditional widely used deblending method that is based on the standard median filtering requires two or three times of velocity scanning and NMO corrections, which is very computationally expensive. Considering the massive field data recorded

from the simultaneous source acquisition, the proposed fast deblending framework can be more practical in efficiently obtaining deblended clean dataset from raw seismic records that are corrupted by intense blending interference. The synthetic and field data examples show that the proposed deblending framework can obtain a similar deblending result compared with the traditional approach but can obtain more than 10 times efficiency improvement. The comparison between migrated results of unblended data, blended data, deblending data using different approaches, further confirms the superior performance of the proposed workflow.

## ACKNOWLEDGEMENTS

The project is supported by the starting fund at North China University of Water Resources and Electric Power.

## REFERENCES

Abma, R., 2014. Shot scheduling in simultaneous shooting. Expanded Abstr., 84th Ann. Internat. SEG Mtg., Denver: 94-98.

Abma, R., Zhang, Q., Arogunmati, A. and Beaudoin, G., 2012. An overview of BPs marine independent simultaneous source field trials. Expanded Abstr., 82nd Ann. Internat. SEG Mtg., Las Vegas: 1-5.

Abma, R.L., T. Manning, M. Tanis, J. Yu, and M. Foster, 2010. High quality separation of simultaneous sources by sparse inversion. Extended Abstr., 72nd EAGE Conf., Barcelona.

Akerberg, P., G. Hampson, J. Rickett, H. Martin, and J. Cole, 2008. Simultaneous source separation by sparse radon transform. Expanded Abstr., 78th Ann. Internat. SEG Mtg., Las Vegas: 2801-2805.

Beasley, C.J., 2008. A new look at marine simultaneous sources. The Leading Edge, 27: 914-917.

Beasley, C.J., R.E. Chambers and Z. Jiang, 1998. A new look at simultaneous sources. Expanded Abstr., 68th Ann. Internat. SEG Mtg., New Orleans: 133-135.

Beasley, C.J., B. Dragoset and A. Salama, 2012. A 3D simultaneous source field test processed using alternating projections. A new active separation method. Geophys. Prosp., 60: 591-601.

Berkhout, A., D. Verschuur and G. Blacquière, 2012. Illumination properties and imaging promises of blended, multiple-scattering seismic data. A tutorial. Geophys. Prosp., 60: 713-732.

Berkhout, A.J., 2008. Changing the mindset in seismic data acquisition. The Leading Edge, 27: 924-938.

Chen, W., J. Yuan, Y. Chen and S. Gan, 2017a. Preparing the initial model for iterative deblending by median filtering. J. Seismic Explor., 26: 25-47.

Chen, Y., 2015a. Deblending using a space-varying median filter. Explor. Geophys., 46: 332-341.

Chen, Y., 2015b. Iterative deblending with multiple constraints based on shaping regularization. IEEE Geosci. Remote Sens. Lett., 12: 2247-2251.

Chen, Y., 2016. Dip-separated structural filtering using seislet thresholding and adaptive empirical mode decomposition based dip filter. Geophys. J. Internat., 206: 457-469.

Chen, Y., 2017, Fast dictionary learning for noise attenuation of multidimensional seismic data. Geophys. J. Internat., 209: 21-31.

Chen, Y., H. Chen, K. Xiang, and X. Chen, 2017b. Preserving the discontinuities in least- squares reverse time migration of simultaneous-source data. Geophysics, 82(3): S185-S196.

Chen, Y. and S. Fomel, 2015. Random noise attenuation using local signal-and-noise orthogonalization. Geophysics, 80(6): WD1-WD9.

Chen, Y., S. Fomel and J. Hu, 2014a. Iterative deblending of simultaneous-source seismic data using seislet-domain shaping regularization. Geophysics, 79: V179-V189.

Chen, Y. and Z. Jin, 2015. Simultaneously removing noise and increasing resolution of seismic data using waveform shaping. IEEE Geosci. Remote Sens. Lett., 13: 102-104.

Chen, Y. and J. Ma, 2014. Random noise attenuation by f-x empirical mode decomposition predictive filtering. Geophysics, 79: V81-V91.

Chen, Y., J. Ma and S. Fomel, 2016. Double-sparsity dictionary for seismic noise attenuation. Geophysics, 81(2): V17-V30.

Chen, Y., J. Yuan, Z. Jin, K. Chen and L. Zhang, 2014b. Deblending using normal moveout and median filtering in common-midpoint gathers. J. Geophys. Engineer., 11: 045012.

Chen, Y., J. Yuan, S. Zu, S. Qu and S. Gan, 2015. Seismic imaging of simultaneous-source data using constrained least-squares reverse time migration. J. Appl. Geophys., 114: 32-35.

Chen, Y., Y. Zhou, W. Chen, S. Zu, W. Huang and D. Zhang, 2017c. Empirical low rank decomposition for seismic noise attenuation. IEEE Transact. Geosci. Remote Sens. doi: 10.1109/TGRS.2017.2698342.

Choi, Y. and T. Alkhalifah, 2012. Application of multi-source waveform inversion to marine streamer data using the global correlation norm. Geophys. Prosp., 60: 748-758.

Doulgeris, P., K. Bube, G. Hampson and G. Blacquière, 2012. Convergence analysis of a coherency-constrained inversion for the separation of blended data. Geophys. Prosp., 60: 769-781.

Ebrahimi, S., A.R. Kahoo, Y. Chen and M.J. Porsani, 2017. A high-resolution weighted ab semblance for dealing with amplitude-variation-with-offset phenomenon. Geophysics, 82(2): V85-V93.

Fomel, S., 2007. Local seismic attributes. Geophysics, 72: A29-A33.

Gan, S., Y. Chen, S. Wang, X. Chen, W. Huang and H. Chen, 2016a. Compressive sensing for seismic data reconstruction using a fast projection onto convex sets algorithm based on the seislet transform. J. Appl. Geophys., 130: 194-208.

Gan, S., Y. Chen, S. Zu, S. Qu and W. Zhong, 2015a. Structure-oriented singular value decomposition for random noise attenuation of seismic data. J. Geophys. Engineer. 12: 262-272.

Gan, S., S. Wang, Y. Chen, J. Chen, W. Zhong and C. Zhang, 2016b, Improved random noise attenuation using f-x empirical mode decomposition and local similarity. Applied Geophysics, 13, 127-134.

Gan, S., S. Wang, Y. Chen and X. Chen, 2016c, Simultaneous-source separation using iterative seislet-frame thresholding. IEEE Geosci. Remote Sens. Lett., 13: 197-201.

Gan, S., S. Wang, Y. Chen, X. Chen and K. Xiang, 2016d. Separation of simultaneous sources using a structural-oriented median filter in the flattened dimension. Comput. Geosci., 86: 46-54.

Gan, S., S. Wang, Y. Chen, S. Qu and S. Zu, 2016e. Velocity analysis of simultaneous-source data using high-resolution semblance-coping with the strong noise. Geophys. J. Internat., 204: 768-779.

Gan, S., S. Wang, Y. Chen, Y. Zhang and Z. Jin, 2015b. Dealiased seismic data interpolation using seislet transform with low-frequency constraint. IEEE Geosci. Remote Sens. Lett., 12: 2150-2154.

Garotta, R., 1983. Simultaneous recording of several vibroseis seismic lines. Expanded Abstr., 53rd Ann. Internat. SEG Mtg., Las Vegas: 308-310.

Guitton, A. and E. Daz, 2012. Attenuating crosstalk noise with simultaneous source full waveform inversion. Geophys. Prosp., 60: 759-768.

Hampson, G., J. Stefani and F. Herkenhoff, 2008. Acquisition using simultaneous sources. Expanded Abstr., 78th Ann. Internat. SEG Mtg., Las Vegas: 2816-2820.

Huang, W., R. Wang, X. Chen and Y. Chen, 2017a. Double least squares projections method for signal estimation. IEEE Transact. Geosci. Remote Sens. doi. 10.1109/TGRS.2017.2688420.

Huang, W., R. Wang, Y. Chen, H. Li and S. Gan, 2016. Damped multichannel singular spectrum analysis for 3D random noise attenuation. Geophysics, 81(4): V261-V270.

Huang, W., R. Wang, Y. Yuan, S. Gan and Y. Chen, 2017b. Signal extraction using randomized-order multichannel singular spectrum analysis. Geophysics, 82(2): V59-V74.

Huo, S., Y. Luo and P.G. Kelamis, 2012. Simultaneous sources separation via multidirectional vector-median filtering. Geophysics, 77: V123-V131.

Ikelle, L., 2007. Coding and decoding. Seismic data modeling, acquisition and processing. Expanded Abstr., 77th Ann. Internat. SEG Mtg., San Antonio: 66-70.

Ikelle, L.T., 2016. Up-down separation of obs wavefield using ica techniques. J. Seismic Explor., 25: 419-432.

Ikelle, L.T., K.-J. Lee and H. Spears, 2000. Multishooting method for simulating seismic surveys. Application to 3D finite-difference modeling. Expanded Abstr., 70th Ann. Internat. SEG Mtg., Calgary: 2209-2212.

Kim, Y., I. Gruzinov, M. Guo and S. Sen, 2009. Source separation of simultaneous source obc data. Expanded Abstr., 79rd Ann. Internat. SEG Mtg., Houston, 51-55.

Kong, D., Z. Peng, Y. He and H. Fan, 2016. Seismic random noise attenuation using directional total variation in the shearlet domain. J. Seismic Explor., 25: 321-338.

Li, H., R. Wang, S. Cao, Y. Chen and W. Huang, 2016a. A method for low-frequency noise suppression based on mathematical morphology in microseismic monitoring. Geophysics, 81(3): V159-V167.

Li, H., R. Wang, S. Cao, Y. Chen, N. Tian and X. Chen, 2016b. Weak signal detection using multiscale morphology in microseismic monitoring. J. Appl. Geophys., 133: 39-49.

Li, Y., Z. Li, K. Zhang and Y. Lin, 2016c. Frequency-domain full waveform inversion with rugged free surface based on variable grid finite-difference method. J. Seismic Explor., 25: 543-559.

Lin, T.T. and F.J. Herrmann, 2009. Designing simultaneous acquisitions with compressive sensing. Extended Abstr., 71st EAGE Conf., Amsterdam.

Liu, C., D. Wang, B. Hu and T. Wang, 2016a. Seismic deconvolution with shearlet sparsity constrained inversion. J. Seismic Explor., 25: 433-445.

Liu, G. and X. Chen, 2013. Noncausal f-x-y regularized nonstationary prediction filtering for random noise attenuation on 3D seismic data. J. Appl. Geophys., 93: 60-66.

Liu, G., X. Chen, J. Du and J. Song, 2011. Seismic noise attenuation using nonstationary polynomial fitting. Appl. Geophys., 8: 18-26.

Liu, W., S. Cao and Y. Chen, 2016b. Application of variational mode decomposition in random noise attenuation and time-frequency analysis of seismic data. Extended Abstr. 78th EAGE Conf., Vienna. doi.10.3997/2214- 4609.201601249.

Liu, W., S. Cao and Y. Chen, 2016c. Applications of variational mode decomposition in seismic time-frequency analysis. Geophysics, 81(5): V365-V378.

Liu, W., S. Cao, Y. Chen and S. Zu, 2016d. An effective approach to attenuate random noise based on compressive sensing and curvelet transform. J. Geophys. Engineer., 13: 135-145.

Liu, W., S. Cao, S. Gan, Y. Chen, S. Zu and Z. Jin, 2016e. One-step slope estimation for dealiased seismic data reconstruction via iterative seislet thresholding. IEEE Geosci. Remote Sens. Lett., 13: 1462-1466.

Liu, W., S. Cao and Y. He, 2015. Ground roll attenuation using variational mode decomposition. Extended Abstr., 77th EAGE Conf., Madrid.

Liu, W., S. Cao, Y. Liu and Y. Chen, 2016f. Synchrosqueezing transform and its applications in seismic data analysis. J. Seismic Explor., 25: 27-44.

Liu, Y., C. Liu and D. Wang, 2009. A 1D time-varying median filter for seismic random, spike-like noise elimination. Geophysics, 74: V17-V24.

Mahdad, A., 2012. Deblending of Seismic Data. Ph.D. thesis, Technical University Delft, Delft, Netherlands.

Mahdad, A., P. Doulgeris and G. Blacquière, 2011. Separation of blended data by iterative estimation and subtraction of blending interference noise. Geophysics, 76: Q9-Q17.

Mahdad, A., P. Doulgeris and G. Blacquière, 2012. Iterative method for the separation of blended seismic data. Discussion on the algorithmic aspects. Geophys. Prosp., 60: 782-801.

Martinez, D.R. and G.A. Crews, 1987. Evaluation of simultaneous vibroseis recording. Expanded Abstr., 57th Ann. Internat. SEG Mtg., New Orleans: 577-580.

Moerig, R., F.J. Barr and D.L. Nyland, 2002. Simultaneous shooting using cascaded sweeps. Expanded Abstr., 72nd Ann. Internat. SEG Mtg., Salt Lake City: 74-76.

Moore, I., 2010. Simultaneous source - processing and applications. Expanded Abstr., 72nd Ann. Internat. SEG Mtg., Salt Lake City.

Moore, I., B. Dragoset, T. Ommundsen, D. Wilson, C. Ward and D. Eke, 2008. Simultaneous source separation using dithered sources. Expanded Abstr., 78th Ann. Internat. SEG Mtg., Las Vegas: 2806-2809.

Qu, S., H. Zhou, H. Chen, S. Zu and L. Zhi, 2014. Separation of simultaneous vibroseis data. Expanded Abstr., 84th Ann. Internat. SEG Mtg., Denver: 4340-4344.

Qu, S., H. Zhou, Y. Chen, S. Yu, H. Zhang, J. Yuan, Y. Yang and M. Qin, 2015. An effective method for reducing harmonic distortion in correlated vibroseis data. J. Appl. Geophys., 115: 120-128.

Qu, S., H. Zhou, R. Liu, Y. Chen, S. Zu, S. Yu, J. Yuan and Y. Yang, 2016. Deblending of simultaneous-source seismic data using fast iterative shrinkage-thresholding algorithm with firm-thresholding. Acta Geophys., 64: 1064-1092.

Ren, C. and X. Tian, 2016. Prestack migration based on asymmetric wave-equation extrapolation. J. Seismic Explor., 25: 375-397.

Shen, H., Y. Yan, C. Chen and B. Zhang, 2016. Multiple-transient surface wave phase velocity analysis in expanded f-k domain and its application. J. Seismic Explor., 25: 299-319.

Siahsar, M.A.N., S. Gholtashi, E. Olyaei, W. Chen and Y. Chen, 2017. Simultaneous denoising and interpolation of 3D seismic data via damped data-driven optimal singular value shrinkage. IEEE Geosci. Remote Sens. Lett. doi.10.1109/LGRS.2017.2697942.

Spitz, S., G. Hampson and A. Pica, 2008. Simultaneous source separation. a prediction- subtraction approach. Expanded Abstr., 78th Ann. Internat. SEG Mtg., Las Vegas: 2811-2814.

Sun, W.,and H. Wang, 2016. Water-layer-related demultiple method using constraints in the sparse, local tau-p domain. J. Seismic Explor., 25: 463-483.

Wapenaar, K., J. van der Neut and J. Thorbecke, 2012. Deblending by direct inversion. Geophysics, 77: A9-A12.

Ward, R., R. Brune, A. Ross and L. Kumamoto, 1990. Phase encoding of vibroseis signals for simultaneous multisource acquisition. Expanded Abstr., 60th Ann. Internat. SEG Mtg., San Francisco: 938-941.

Werner, H., 1993. Application of vibroseis simultaneous multiple source recording. Expanded Abstr., 63rd Ann. Internat. SEG Mtg., Washington D.C.: 569-571.

Womack, J.E. and J.R. Cruz, 1988. Simultaneous vibroseis encoding techniques. Expanded Abstr., 58th Ann. Internat. SEG Mtg., Anaheim: 101-104.

Wood, L.C., 1974. Seismic data compression methods. Geophysics, 39: 499-525.

Wu, J., R. Wang, Y. Chen, Y. Zhang, S. Gan and C. Zhou, 2016. Multiples attenuation using shaping regularization with seislet domain sparsity constraint. J. Seismic Explor., 25: 1-9.

Xue, Y., F. Chang, D. Zhang and Y. Chen, 2016a. Simultaneous sources separation via an iterative rank-increasing method. IEEE Geosci. Remote Sens. Lett., 13: 1915-1919.

Xue, Y., M. Man, S. Zu, F. Chang and Y. Chen, 2017. Amplitude-preserving iterative deblending of simultaneous source seismic data using high-order radon transform. J. Appl. Geophys., 139: 79-90.

Xue, Y., J. Yang, J. Ma and Y. Chen, 2016b. Amplitude-preserving nonlinear adaptive multiple attenuation using the high-order sparse radon transform. J. Geophys. Engineer., 13: 207-219.

Xue, Z., Y. Chen, S. Fomel and J. Sun, 2016c. Seismic imaging of incomplete data and simultaneous-source data using least-squares reverse time migration with shaping regularization. Geophysics, 81: S11-S20.

Yang, W., R. Wang, Y. Chen, J. Wu, S. Qu, J. Yuan and S. Gan, 2015a. Application of spectral decomposition using regularized non-stationary autoregression to random noise attenuation. J. Geophys. Engineer., 12: 175-187.

Yang, W., R. Wang, J. Wu, Y. Chen, S. Gan and W. Zhong, 2015b. An efficient and effective common reflection surface stacking approach using local similarity and plane-wave flattening. J. Appl. Geophys., 117: 67-72.

Zhang, D., Y. Chen, W. Huang and S. Gan, 2016a. Multi-step damped multichannel singular spectrum analysis for simultaneous reconstruction and denoising of 3D seismic data. J. Geophys. Engineer., 13: 704-720.

Zhang, H., J. Xu, Q. Liu and J. Zhang, 2016b. Imaging 2d rugged topography seismic data. A topography pstm approach integrated with residual static correction. J. Seismic Explor. 25: 339-358.

Zhong, W., Y. Chen, S. Gan, and J. Yuan, 2016, $L_{1/2}$ norm regularization for 3D seismic data interpolation. J. Seismic Explor., 25: 257-268.

Zhou, Y., 2017. A POCS method for iterative deblending constrained by a blending mask. J. Appl. Geophys., 138: 245-254.

Zhou, Y., C. Shi, H. Chen, J. Xie, G. Wu and Y. Chen, 2017. Spike-like blending noise attenuation using structural low-rank decomposition. IEEE Geosci. Remote Sens. Lett., 14. doi.10.1109/LGRS.2017.2687418.

Zu, S., H. Zhou, Y. Chen, X. Pan, S. Gan and D. Zhang, 2016a. Interpolating big gaps using inversion with slope constraint. IEEE Geoscience and Remote Sensing Lett., 13,: 1369-1373.

Zu, S., H. Zhou, Y. Chen, S. Qu, X. Zou, H. Chen and R. Liu, 2016b. A periodically varying code for improving deblending of simultaneous sources in marine acquisition. Geophysics, 81: P1-13.